MODELING OF DENSE REACTIVE GRANULAR FLOWS[1]

Danny Lathouwers[†]* and Josette Bellan**[2]
Jet Propulsion Laboratory, California Institute of Technology, Pasadena, California, 91109-8099
[†]Interfaculty Research Institute (IRI), Delft University of Technology. Mekelweg 15, Delft, The Netherlands.

Abstract

A general model of dense granular flows derived elsewhere is here assessed to understand the validity of some of the assumptions embedded in the derivation. The isothermal hydrodynamic model has been validated elsewhere, however, due to the new addition of the heat transfer (both convective and radiative) and reaction models, it is deemed important to again evaluate the model assumptions and see if they hold under this more complex situation. The separately validated hydrodynamic model is based on a three fluid model (gas, sand, and biomass) derived from the kinetic theory of granular flows. Separate transport equations are constructed for each particle class, allowing for the calculation of the granular stresses, granular conductivities and granular viscosities, and enabling the description of such phenomena as particle segregation and the evolution of separate temperatures for each particle class. A previously validated biomass particle pyrolysis model is coupled with the detailed hydrodynamic model for the binary gas particle mixture. The kinetics scheme is based on superimposed cellulose, hemicellulose, and lignin reactions enabling the simulation of any biomass feedstock whose initial mass composition with respect to these three primary components is known. Using results of simulations, we assess *a posteriori* one modeling and one computational assumption pertaining to the granular stresses and the granular conductivities, respectively. Further we also investigate the accuracy of the particle heating model.

Introduction

The interest in clean hydrogen fuel production has triggered substantial activity in high temperature biomass pyrolysis for the purpose of obtaining a process that maximizes tar yield while simultaneously minimizing char formation. Biomass pyrolysis involves the heating of raw biomass in the absence of an oxidizer in order to extract reaction products for subsequent processing. Among several reactor geometries, the vortex reactor and the fluidized bed reactor were the subject of research activities at the National Renewable Energy Laboratory (NREL), being potentially attractive as commercial pyrolysis devices. The vortex reactor was the subject of an earlier study (Miller and Bellan [17]) accomplished by coupling a detailed model for pyrolysis to a fundamental fluid dynamics model of the vortex reactor. A similarly fundamental and detailed study of the pyrolysis conditions in a bubbling fluidized bed is not available in the literature.

The fluidized bed reactor consists of a cylindrical vessel partially filled with sand whose main purpose is to provide a large heat reservoir to keep the mean temperature of the bed constant. Fresh, relatively cool, biomass is injected into the reactor through a feeding mechanism in the wall, or directly into the bed using an injection 'rod'. Since pyrolysis is an endothermic process, heat is provided to the biomass by heating the walls of the reactor and by injecting hot steam or nitrogen which is further used to fluidize the mixture, while also preheating it. The fluidizing gas induces a gas and solid flow pattern in the reactor, with both locally dense and void particle regions. An overall circulative complex flow occurs, explaining the excellent mixing behavior of fluidized bed reactors. Following introduction in the reactor, the biomass partially mixes with the sand and heats up. As heating progresses, the particles pyrolyze and eject product gases (tar and gas; gas denotes here the collection of gaseous products complementary to tar) while simultaneously forming char which maintains the particle matrix. Product gases mix up with the fluidizing gas and are transported towards the reactor exit after which they are cooled to prevent product degradation, making collection of the condensable tars possible.

To describe the complex granular flow in this reactor, Lathouwers and Bellan [13] have developed a fundamental model accounting for the different history of the two particle classes represented by the sand and biomass, and for the interaction between gas and particles. This isothermal model has been validated with data available in the literature [13]. The new addition by Lathouwers and Bellan [14] of the heat transfer model and the validated kinetic scheme of Miller and Bellan [16] warrants a re-evaluation of the assumptions used to derive the hydrodynamic model, as well as an *a posteriori* assessment of the heat transfer model assumptions. This paper describes an examination of important assumptions used in this model.

Model formulation

The model previously developed by Lathouwers and Bellan [14] consists of coupled submodels of the biomass kinetics and of the hydrodynamics of the gas particle mixture. The succinct description of these submodels is addressed below.

Single particle biomass pyrolysis model

The adopted particle pyrolysis model is that of the detailed kinetics derived by Miller and Bellan [16], based on superimposed cellulose, hemicellulose, and lignin reactions. This model enables the simulation of different biomass feedstock through knowledge of the initial mass composition with respect to these three primary components; biomass impurities are lumped with the hemicellulose as this model correlated best with the experimental data. Each of the virgin components undergoes the

[2] *Research Scientist; **Senior Research Scientist, Associate AIAA Fellow (corresponding author, josette.bellan@jpl.nasa.gov).

same generic competitive reaction scheme:

$$\begin{aligned}
&\text{virgin}(s) \xrightarrow{K_1} \text{active}(s) \\
&\text{active}(s) \xrightarrow{K_2} \text{tar}(g) \\
&\text{active}(s) \xrightarrow{K_3} X\text{char}(s) + (1-X)\text{gas}(g) \\
&\text{tar}(g) \xrightarrow{K_4} \text{gas}(g).
\end{aligned} \tag{1}$$

As indicated in the above kinetic scheme by the letter in parenthesis, the virgin components, the active intermediates and the char are solid phase species, while tar and gas are vapor products; none of these species are pure chemical species, but instead represent groups of compounds. All reactions are modelled with first order Arrhenius kinetics: $K_i = A_i \exp(-E_i/RT)$, where the rate constants, A_i, activation energies, E_i for reactions K_1, K_2, K_3 and the mass ratio X are dependent on the particular component, whereas all heats of reaction and secondary tar decomposition parameters (K_4) are independent of the source component. The kinetic parameters are specified in Table 1. The depolymerization reaction K_1 has Δh_1 =0 kJ/kg, reaction K_2 is endothermic with Δh_2 =255 kJ/kg, and both the char formation and the secondary tar reactions are exothermic with $\Delta h_2 = -20$ kJ/kg and $\Delta h_2 = -42$ kJ/kg. All other properties of gaseous and solid species are listed in Tables 2 and 3, respectively.

In Miller and Bellan [16], this kinetic model combined with a porous particle flow dynamics model yielded validated predictions on tar/char yields ranging from the kinetically controlled regime (micro particles) to the diffusion controlled limit (macro particles). In the present model, for simplicity, the biomass pyrolysis is assumed kinetically controlled. This is consistent with the further assumption (see below) of small Biot number.

Hydrodynamic model

The hydrodynamic model describing the dynamics of the gas particle mixture is that derived by Lathouwers and Bellan [13]. Here, we give a brief description of the model, referring the reader for full details to the derivation of Lathouwers and Bellan [14].

The model is based on a three fluid model description where macroscopic transport equations are derived from the kinetic theory of granular flows using inelastic sphere models, thereby accounting for collisional transfer in high density regions. Separate transport equations are constructed for each of the particle classes, allowing for the independent acceleration of the particles in each class and the interaction between size classes.

Definitions and averaging

The continuum model was derived by Lathouwers and Bellan [14] applying separate averaging procedures to both the carrier gas and solid phases. A phase ensemble average was used for the carrier phase, combined with a particle ensemble average where particle properties, such as velocity, are directly averaged.

The general ensemble average of a field quantity $\Psi(\mathbf{x},t)$, ($\mathbf{x}, t$ denoting space and time coordinates) is

$$< \Psi(\mathbf{x},t) >= \int \Psi(\mathbf{x},t) P(\Pi) d\Pi \tag{2}$$

where $P(\Pi)$ is the probability that a specific realization Π is encountered in the ensemble. The gas-phase ensemble average and its density-weighted counterpart are defined (Drew [6]) as $\overline{\Psi} \equiv < \chi_g \Psi(\mathbf{x},t) > /\alpha_g$ and $\widetilde{\Psi} \equiv < \chi_g \rho_g \Psi(\mathbf{x},t) > /\alpha_g \overline{\rho}_g$, where ρ_g is the gas density, χ_g denotes the phase indicator of the gas phase which is unity in the gas phase and zero otherwise, and the gas phase fraction, α_g, is defined as the ensemble average of the indicator function, i.e. $\alpha_g =< \chi_g >$.

The transport equations for the solids were derived similarly to those for dense gases, using kinetic theory concepts.

Let $f_i^{(1)}(\mathbf{x}, \mathbf{c}, Y_\xi, T, m, t)$ denote the single particle distribution function of particle class i such that $f_i^{(1)}$ is the probable number of particles of class i having their center of mass in the region $[\mathbf{x}, \mathbf{x}+d\mathbf{x}]$, a velocity in the region $[\mathbf{c}, \mathbf{c}+d\mathbf{c}]$, mass in the region $[m, m+dm]$, mass fractions in $[Y_\xi, Y_\xi + dY_\xi]$, and temperature in $[T, T+dT]$. With this distribution function, a particle average is introduced as an integration over the phase space

$$\overline{\Psi}_i(\mathbf{x},t) = \frac{1}{n_i} \int \Psi_i f_i d\mathbf{c} dY_\xi dT dm. \tag{3}$$

Here n_i denotes the number density of the solid class i, and is defined as

$$n_i(\mathbf{x},t) = \int f_i d\mathbf{c} dY_\xi dT dm. \tag{4}$$

It is also convenient to introduce mass weighted averages

$$\widetilde{\Psi}_i(\mathbf{x},t) = \frac{1}{\alpha_i \overline{\rho}_i} \int m_i \Psi_i f_i d\mathbf{c} dY_\xi dT dm \tag{5}$$

where $\alpha_i \overline{\rho}_i = n_i \overline{m}_i = \int m_i f_i d\mathbf{c} dY_\xi dT dm$.

Here, α_i denotes the local phase fraction of class i (where pores are excluded, i.e. are counted as part of the gas phase) and $\overline{\rho}_i$ its corresponding average particle density. We also introduce equivalent definitions for $\widehat{\alpha}_i$ and $\widehat{\rho}_i$ where the pores of the particles are counted as volume belonging to the particle. Note that $\alpha_i \overline{\rho}_i = \widehat{\alpha}_i \widehat{\rho}_i$. Mass weighted averages are also denoted by brackets, i.e. $< \Psi >_i \equiv \widetilde{\Psi}_i$ in the equations below. Using the above definitions we define the average velocity $\mathbf{u}_i =< \mathbf{c}_i >$, the fluctuation velocity component, $\mathbf{C}_i = \mathbf{c}_i - \mathbf{u}_i$, and the granular temperature, $\Theta_i = \frac{1}{3} < C_i^2 >$. The granular temperature plays a crucial role in the determination of the transport properties of granular flows and may be interpreted similarly to the temperature of a normal gas (see e.g. Campbell [4]).

The solidity of a particle, $\eta = 1 - \epsilon$, where ϵ is the porosity of a particle, is defined as the ratio of the volume displaced by the particle and the volume displaced by the particle had its pores been closed. The solidity is then easily shown to equal

$$\eta_i = \frac{m_i}{V_i} \sum \frac{Y_\xi}{\rho_\xi} \tag{6}$$

where V_i is the total volume of a particle (including its pores). In the present case of biomass pyrolysis, we assume that the

particle diameter stays constant throughout the pyrolysis, and that the porosity of the particle simply increases in time (Miller and Bellan [16]). This assumption is correct when the particle does not break or erodes.

Macroscopic equations

Applying the averaging formalism to the gas phase equations, one obtains the macrospcopic equations.

Mass: The mass conservation equation for the gas phase is

$$\frac{\partial(\alpha\overline{\rho})_g}{\partial t} + \nabla\cdot(\alpha\overline{\rho}\widetilde{\mathbf{u}})_g = \Gamma_g \tag{7}$$

where α, ρ, and $\mathbf{u}$ denote the volume fraction, density and velocity respectively. The term on the right hand side, Γ_g, represents the mass transfer rate originating from pyrolysis.

Similar equations can be derived for each solid class i through the formalism stated earlier:

$$\frac{\partial(\alpha\overline{\rho})_i}{\partial t} + \nabla\cdot(\alpha\overline{\rho}\mathbf{u})_i = \Gamma_i \tag{8}$$

where the mass transfer rate for each solid class is related to the average mass reduction of all particles in the specific class, $\Gamma_i = \alpha_i\overline{\rho}_i < \frac{1}{m_i}\frac{dm_i}{dt} >$.

Momentum: The gas phase momentum equation can be written as

$$\frac{\partial(\alpha\overline{\rho}\widetilde{\mathbf{u}})_g}{\partial t} + \nabla\cdot(\alpha\overline{\rho}\widetilde{\mathbf{u}}\widetilde{\mathbf{u}})_g = -\alpha_g\nabla\overline{p}_g + \nabla\cdot 2\alpha_g\mu_g\mathbf{S}_g + \tag{9}$$
$$\alpha_g\overline{\rho}_g\mathbf{f}_g + \sum_i \frac{\alpha_i\overline{\rho}_i}{\tau_{i,12}}(\mathbf{u}_i - \widetilde{\mathbf{u}}_g) - \sum_i \Gamma_i\mathbf{u}_i$$

where p_g is the thermodynamic pressure, $\mathbf{S}_g$ denotes the strain rate tensor $\mathbf{S}_g = (\nabla\widetilde{\mathbf{u}}_g + \nabla\widetilde{\mathbf{u}}_g^T)/2 - (\nabla\cdot\widetilde{\mathbf{u}}_g)/3$, μ_g is the shear viscosity, $\mathbf{f}_g$ is the gravitational acceleration and $\tau_{i,12}$ is the interaction time scale between fluid and particle. The terms on the right hand side denote the pressure gradient force, shear stresses, gravitational body force, the force exerted on the gas phase by drag on the particles and finally, the effect of mass transfer on the momentum of the carrier gas.

$\tau_{i,12}$ depends strongly on the flow regime; in the dilute regime it is derived from the drag coefficient, C_d, of a single particle in an infinite medium, empirically corrected for the presence of other surrounding particles by a function $f(\alpha_g) = \widehat{\alpha}_g^{-1.7}$ (e.g. Gidaspow [7]), whereas in the dense regime the classical Ergun relation is used. To avoid discontinuous behavior, a weighted average of the two time scales is introduced

$$\frac{1}{\tau_{i,12}} = W\frac{3\overline{\rho}_g C_d(Re_i)}{4\overline{\rho}_i d_i}|\mathbf{u}_i - \widetilde{\mathbf{u}}_g| f(\widehat{\alpha}_g) + \tag{10}$$
$$(1-W)\frac{\overline{\rho}_g}{\overline{\rho}_i}\left[(1-\widehat{\alpha}_g)\frac{150}{Re_i} + 1.75\right]\frac{|\mathbf{u}_i - \widetilde{\mathbf{u}}_g|}{d_i}$$

where the present switch function, $W(\widehat{\alpha}_g) = \arctan(150(\widehat{\alpha}_g - 0.8))/\pi + 1/2$, gives a rapid transition from one regime to the other. d_i is the diameter of the particle and Re_i is the Reynolds number based on the relative velocity with the gas, $Re_i = \widehat{\alpha}_g\rho_g|\mathbf{u}_i - \widetilde{\mathbf{u}}_g|d_i/\mu_g$. The single particle drag coefficient C_d is determined from the well-known correlation (Schiller and Nauman [19]) $C_d = \frac{24}{Re_i}(1 + 0.15Re_i^{0.687})$.

The averaged momentum equation for each solids class is

$$\frac{\partial(\alpha\overline{\rho}\widetilde{\mathbf{u}})_i}{\partial t} + \nabla\cdot(\alpha\overline{\rho}\widetilde{\mathbf{u}}\widetilde{\mathbf{u}})_i = -\widehat{\alpha}_i\nabla\overline{p}_g - \nabla\cdot(\Sigma_i + \Sigma_i^f) \tag{11}$$
$$+ \alpha_i\overline{\rho}_i\mathbf{f}_g + \frac{\alpha_i\overline{\rho}_i}{\tau_{i,12}}(\widetilde{\mathbf{u}}_g - \mathbf{u}_i)$$
$$+ \phi_i + \Gamma_i\mathbf{u}_i.$$

This equation contains similar terms when compared to its gas phase counterpart, i.e. a mean pressure gradient, a drag term having the reverse sign compared to that in the gas phase equation, and a mass transfer related term. Terms unique to the solid's equation are the solid stress tensors, Σ_i and Σ_i^f, and a collisional source term, ϕ_i which represents the momentum exchange among the various solid classes due to collisions. Closure relations for these terms, derived by Lathouwers and Bellan [14], are provided below.

For application in the dense regime, a frictional stress term, Σ_i^f, is added. The proposed model consists of a simple relationship between stresses and strains: $\Sigma_i^f = -p_i^f\mathbf{I} + 2\mu_i^f\mathbf{S}_i$ for $\alpha > \alpha_{min}$ where α_{min} is the minimum solids fraction at which frictional transfer becomes influential. Experimental observations indicate that the frictional normal stress increases rapidly with bulk density and diverges as α_{max} is approached. A simple algebraic representation of this behavior is (c.f. Anderson and Jackson [1])

$$p_i^f = \frac{\alpha_i\rho_i}{\sum\alpha_i\rho_i}Fr\frac{(\widehat{\alpha} - \alpha_{min})^p}{(\alpha_{max} - \widehat{\alpha})^n} \tag{12}$$

where Fr is a material constant. The frictional viscosity, μ_i^f, is related to the frictional pressure and the angle of internal friction, ϕ, as $\mu_i^f = p_i^f\sin(\phi)/2\sqrt{I_2}$ where I_2 denotes the second invariant of the strain rate tensor. The following values for the parameters have been used in the present work: $p = 2$, $n = 5$, $Fr = 0.005$, $\alpha_{min} = 0.6$, $\alpha_{max} = 0.64$, and $\phi = 25$ degrees (see [1] and [13]).

Species: The gas phase species equations is

$$\frac{\partial(\alpha\overline{\rho}\widetilde{Y}_\xi)_g}{\partial t} + \nabla\cdot(\alpha\overline{\rho}\mathbf{u}\widetilde{Y}_\xi)_g = \nabla\cdot\alpha_g\overline{\rho}_g\mathcal{D}_\xi\nabla\widetilde{Y}_{g\xi} \tag{13}$$
$$+\alpha_g\overline{\rho}_g\widetilde{R}_{g\xi} + \sum_i\alpha_i\overline{\rho}_i < R_{i,\xi}^{s\rightarrow g} >$$

The first term on the right hand side represents molecular diffusion and $\mathcal{D}_\xi$ is the diffusion coefficient; the second term is the average production rate of specie ξ due to gas phase reaction; whereas the final term denotes the mass source for a particular component due to solid's reactions, converting solids to gas.

For the species in each solid class, a similar equation is

obtained

$$\frac{\partial(\alpha\overline{\rho}\widetilde{Y}_\xi)_i}{\partial t} + \nabla\cdot(\alpha\overline{\rho}\mathbf{u}\widetilde{Y}_\xi)_i = \nabla\cdot(\alpha_i\overline{\rho}_i\mathcal{D}_{ii}\nabla\widetilde{Y}_{i\xi}) + \Gamma_{i\xi}. \tag{14}$$

The first term on the right hand side denotes the diffusion of species due to fluctuations in the velocity of the solids. $\mathcal{D}_{ii}$ is calculated as the self diffusion coefficient which is directly derived from the velocity distribution of the particles (see Lathouwers and Bellan [14] for a detailed derivation). The second term, $\Gamma_{i\xi} = \alpha_i\overline{\rho}_i < R_{i,\xi} >$ is the average mass source arising from the pyrolysis reactions.

Thermal energy: The thermal energy equation for the gas phase is

$$(\alpha\overline{\rho}C_p)_g\frac{D_g\widetilde{T}_g}{Dt} = \nabla\cdot\alpha_g\lambda_g\nabla\widetilde{T}_g + \sum_i\frac{6\widehat{\alpha}_i\lambda_g}{d_i^2}Nu_i(\widetilde{T}_i - \widetilde{T}_g) \tag{15}$$
$$+\sum_i\{\Gamma_{tar}^{s\to g}(C_p^{tar}\widetilde{T}_b - C_{p,g}\widetilde{T}_g) + \Gamma_{gas}^{s\to g}(C_p^{gas}\widetilde{T}_i - C_{p,g}\widetilde{T}_g)\}.$$

The first term on the right hand side is the thermal conductive flux where λ_g is the thermal conductivity. The second term represents the heat exchange with the particles by conduction and convection; Nu_i denotes the effective Nusselt number associated with this transfer. The final collection of terms is the excess enthalpy flux entering the gas phase carried by the gaseous products leaving the particles, where it is assumed that the vapor products leave the particle at its mean temperature. $\Gamma_{tar}^{s\to g}$, and $\Gamma_{gas}^{s\to g}$ denote the averaged mass transfer rates of respectively, tar and gas.

In the present case, the Nusselt number is given by the single particle Nusselt relation, multiplied by a correction factor, F_{bl}, accounting for the effect of mass transfer on the heat transfer rate, i.e.

$$Nu = Nu_0F_{bl}(Re_{bl}, Pr_g). \tag{16}$$

The formulation used here for the blowing factor is that taken from Miller et al.[18] and was also given by Gyarmathy [9] where the factor depends on the 'blowing Reynolds number', $Re_{bl} = \dot{m}/\pi d_i\mu_g$,

$$F_{bl} = \frac{Pr_gRe_{bl}/2}{e^{Pr_gRe_{bl}/2} - 1}. \tag{17}$$

The necessity of this blowing factor correction will be evaluated below on an *a posteriori* basis. To calculate Nu_0, we use the standard Ranz correlation: $Nu_0 = 2 + 0.66Re_i^{1/2}Pr_g^{1/3}$.

The final enthalpy equation for each solid class is

$$(\alpha_i\overline{\rho}C_p)_i\frac{D_i\widetilde{T}_i}{Dt} = \nabla\cdot(\alpha_i\overline{\rho}_iC_{p,i}\mathcal{D}_{ii}\nabla\widetilde{T}_i) + \tag{18}$$
$$\frac{6\widehat{\alpha}_i\lambda_g}{d_i^2}Nu_i(\widetilde{T}_g - \widetilde{T}_i) + \alpha_i\overline{\rho}_i < \frac{Q_{r,i}}{m_i} > + \alpha_i\overline{\rho}_i < \frac{dm_i}{dt}\frac{(h_v - \widetilde{h}_i)}{m_i} > .$$

The second term on the right hand side is also present in the gas phase equation, and was discussed above. The term $\alpha_i\overline{\rho}_i < Q_{r,i}/m_i >$ denotes the source due to thermal radiation processes which is modeled through a six-flux method (see Zaichik et al. [24] and Lathouwers and Bellan [14]).

The final term on the right hand side of eq. 18 is exactly equal to the total average heat of reaction of all reactions taking place in the particle (both solid to solid and solid to gas).

Granular kinetic energy: The transport equation for the granular temperature of each particle class is

$$\frac{3}{2}[\frac{\partial(\alpha\overline{\rho}\Theta)_i}{\partial t} + \nabla\cdot(\alpha\overline{\rho}\widetilde{\mathbf{u}}\Theta)_i] = -\Sigma_i : \nabla\widetilde{\mathbf{u}}_i - \nabla\cdot\mathbf{q}_i + \gamma_i + \frac{3}{2}\Gamma_i\Theta_i. \tag{19}$$

The first term on the right hand side of eq. 19 is the production of kinetic energy of the fluctuations due to shearing of the solid phase. $\mathbf{q}_i$ is the average 'heat flux' both due fluctuations in the velocity of the particles and through collisions. The source term, γ_i, represents the effects of energy redistribution among particle classes and the dissipative effect of inelastic collisions. The effect of mass transfer is contained in the last term of eq. 19.

Collisional and kinetic contributions: The single particle distribution function is assumed to be Maxwellian, i.e. the lowest order approximation to the Boltzmann equation in the absence of dissipative effects

$$f_i^{(1)}(\mathbf{x}, \mathbf{c}_i, t) = \frac{n_i}{(2\pi\Theta_i)^{3/2}}\exp[\frac{-(\mathbf{c}_i - \widetilde{\mathbf{u}}_i)^2}{2\Theta_i}]. \tag{20}$$

This is a good approximation when the flow has small spatial gradients, the collisions are nearly elastic and the particles are sufficiently heavy (i.e. the time between collisions is much smaller than the particle relaxation time; the particle-fluid correlation is small).

The collision integrals require specification of the radial distribution function at contact, $h_{ik}(\mathbf{r})$, accounting for the effects of excluded area and particle shielding on the spatial distribution of colliding pairs. The form of the radial distribution function is taken from Jenkins and Mancini [10], slightly adjusted to prevent overpacking of the solids, α_{max} being the

maximum allowable solids volume fraction

$$h_{ik} = \frac{1}{1-\widehat{\alpha}/\alpha_{max}} + 6\frac{\sigma_i\sigma_k}{\sigma_i+\sigma_k}\frac{\xi}{(1-\widehat{\alpha}/\alpha_{max})^2} + 8\left(\frac{\sigma_i\sigma_k}{\sigma_i+\sigma_k}\right)^2\frac{\xi}{(1-\widehat{\alpha}/\alpha_{max})^3}. \quad (21)$$

Here $\xi = 2\pi/3\sum n_i\sigma_i^2$ where σ_i denotes the radius of a particle of class i.

The present study is targeted towards dense systems where the drift between particle classes is small; this assumption will be evaluated below. Under this assumption, the collision integrals are approximated by assuming that the relative velocity $\Delta\mathbf{u}_{ik} = \mathbf{u}_i - \mathbf{u}_k$, is small compared to the square root of the sum of the granular temperatures, $(\Theta_i + \Theta_k)^{1/2}$. A more detailed discussion may be found in Lathouwers and Bellan [14].

Using the above distributions and neglecting products of the spatial gradients, products of $(1 - e_{ik})$ with spatial gradients where e_{ik} is the restitution coefficient, and products of $\Delta\mathbf{u}_{ik}$ with the spatial gradients, yields the following constitutive equations for ϕ_i, Σ_i, $\mathbf{q}_i$, and γ_i

$$\phi_i = \sum_k F_{ik}\{\frac{4}{3}\sqrt{2\pi}(\Theta_i+\Theta_k)^{1/2}(\widetilde{\mathbf{u}}_k - \widetilde{\mathbf{u}}_i) + \frac{\pi}{3}\sigma_{ik}(\Theta_i+\Theta_k)\nabla\ln\frac{n_i}{n_k}\} \quad (22)$$

$$\Sigma_i = n_i m_i\Theta_i\mathbf{I} + \sum_k\{p_{ik}\mathbf{I} - \mu_i^{ik}[2\mathbf{S}_i + \frac{5}{3}\nabla\cdot\widetilde{\mathbf{u}}_i] - \mu_i^{kk}[2\mathbf{S}_k + \frac{5}{3}\nabla\cdot\widetilde{\mathbf{u}}_k]\} \quad (23)$$

$$\mathbf{q}_i = \sum_k\{\kappa_i^{ik}\nabla\Theta_i + \kappa_i^{kk}\nabla\Theta_k\} \quad (24)$$

$$\gamma_i = \sum_k -2\sqrt{2\pi}F_{ik}(\Theta_i+\Theta_k)^{1/2}\{2(M_i\Theta_i - M_k\Theta_k) + M_k(1-e_{ik})(\Theta_i+\Theta_k)\} \quad (25)$$

where $F_{ik} = n_i n_k m_i M_k(1+e_{ik})h_{ik}\sigma_{ik}^2$. The indices on the viscosities and conductivities are arranged as follows: the subscript i indicates the relevance for class i, the first superscript labels the pertinent velocity gradient, and the k superscript denotes the collisions with particles from class k. The granular pressure and granular transport coefficients are

$$p_{ik} = \frac{1}{3}\pi n_i n_k m_i M_k(1+e_{ik})h_{ik}\sigma_{ik}^3(\Theta_i+\Theta_k) \quad (26)$$

$$\mu_i^{ik} = \frac{1}{15}\sqrt{2\pi}n_i n_k m_i M_k^2(1+e_{ik})h_{ik}\sigma_{ik}^4(\Theta_i+\Theta_k)^{3/2}/\Theta_i \quad (27)$$

$$\mu_i^{kk} = \frac{1}{15}\sqrt{2\pi}n_i n_k m_k M_i^2(1+e_{ik})h_{ik}\sigma_{ik}^4(\Theta_i+\Theta_k)^{3/2}/\Theta_k \quad (28)$$

$$\kappa_i^{ik} = \frac{1}{3}\sqrt{2\pi}n_i n_k m_i M_k(1+e_{ik})h_{ik}\sigma_{ik}^4(\Theta_i+\Theta_k)^{1/2}\times (M_k\Theta_k/\Theta_i) \quad (29)$$

$$\kappa_i^{kk} = \frac{1}{3}\sqrt{2\pi}n_i n_k m_i M_k(1+e_{ik})h_{ik}\sigma_{ik}^4(\Theta_i+\Theta_k)^{1/2}\times (M_i\Theta_i/\Theta_k). \quad (30)$$

The terms in ϕ_i represent solid-solid drag and ordinary diffusion, respectively (thermal diffusion has been neglected). For coding purposes, the shear rates of both phases are assumed equal (small drift) so that the actually used viscosity equals the sum of several contributions: $\mu_i = \sum_k \mu_i^{ik} + \mu_i^{kk}$. A similar procedure has been used for the conductivity. This computational assumption avoids the appearance of cross derivatives in the granular energy equation, thereby simplifying the discretization and rendering the computations more efficient. This computational assumption will be assessed below.

Auxiliary relations To account for the spatio-temporal distribution of the mass of the biomass particles, the following transport equation for the mean particle mass of each reactive solid is solved:

$$\frac{\partial(\alpha\overline{\rho m})_i}{\partial t} + \nabla\cdot(\alpha\overline{\rho}\widetilde{\mathbf{u}}\overline{m})_i = \nabla\cdot\alpha_i\overline{\rho}_i\mathcal{D}_{ii}\nabla\overline{m}_i - 2\Gamma_i\overline{m}_i. \quad (31)$$

Initial and boundary conditions

Initial conditions are specified corresponding to the standard fluid bed sketched in Fig. 1. Although the real fluidized bed is a cylindrical vessel, for computational simplicity, the present computational domain is approximated to be rectangular with coordinates (x, y). The fluid bed is initially at rest, having specified the velocities of all phases to be null; the granular energy is set to a small number, typically $10^{-7}m^2/s^2$. To induce bubbling, several void areas are created at the bottom of the bed by setting the void fraction to unity in specified computational cells. Practically, there are three such regions distributed on the x axis, at locations corresponding to cells 5-7, 18-20 and 30-32. Areas are then created by making these regions 5 computational cells high in the y direction. The effects of the initial conditions survive a minute fraction of the total physical time and do not affect the statistical behavior of the fluid flow.

Inflow conditions are specified to reflect realistic conditions corresponding to bubbling fluidization; at inlet sections, the volume fractions and velocities are specified together with the temperatures of all phases and the composition of the gas phase and biomass particles, depending on the pertinent feedstock used. The initial temperature of both sand and gas in the domain is set equal to the inlet temperature of the fluidization gas. Hence, it is assumed that the fluidization gas has preheated the sand, even though initially the sand bed is stationary. This does not affect the calculation of product yield, as we are interested in the asymptotic (i.e. long time) behavior of the reactor; that is, long after which a statistically steady flow field has emerged.

Along solid walls, no-slip conditions are applied for the gas phase ($\tilde{\mathbf{u}}_g = 0$), whereas the solids are allowed to slip freely ($\partial \tilde{\mathbf{u}}_{s,t}/\partial n = 0$, where n is a unit normal and the subscript t denotes tangential). Zero-flux boundary conditions are imposed for the solids thermal energy equations, consistent with the energy transfer in particle wall collisions being negligible. As the thermal boundary layers along the wall are not resolved, a similar condition is imposed for the gas phase.

At outlets, Neumann conditions are specified for all variables. Solids are inhibited to exit the domain, simulating a fine solids-filtering grid.

Numerical procedure

Spatial discretization of the governing equations is based on a finite volume technique using a staggered grid. All convective fluxes are approximated with a second-order accurate bounded TVD-scheme. The time discretization is based on a backward Euler scheme in combination with a pressure-correction technique. The momentum equations of all phases are solved in a coupled manner, though separately for each velocity direction. Compared with the well-known Partial Elimination Algorithm (PEA), the present approach is more general (see Lathouwers [11] for more details on full-field coupling and multiphase pressure correction algorithms). The species and energy equations constitute a strongly coupled, stiff system of equations. To avoid very large linear systems arising from (the necessarily) implicit discretization, a time splitting is used (Strang [23]) for the combined species and energy system consisting of three steps: (i) performance of a half convection-diffusion time step, (ii) time integration of the equations over a full time step with only the source terms present (reaction terms, radiation, etc.), (iii) performance of another half convection-diffusion time step. The advantage of this split scheme is that during steps (i) and (iii), the equations are decoupled into standard convection-diffusion systems which are easily handled, whereas in step (ii) there is no spatial coupling. The stiff integration in step (ii) is performed by using the well-known stiff integrator VODE (Brown et al. [3]). All sparse linear systems arising from the discretization of convection-diffusion systems are solved with preconditioned Krylov methods (Conjugate Gradient (CG) for the pressure Poisson equation and Generalized Minimum RESidual (GMRES) for the other transport equations; see e.g. Barrett et al. [2]).

All computations have been performed on a 40×148 uniform grid (x and y directions respectively). Runs have been performed in parallel (although the code is serial) on a SGI Origin 2000 supercomputer. Simulation of 5 seconds of physical time requires approximately 250 hours of CPU time per run.

Biomass particle pyrolysis in a fluidized bed reactor

Among the pyrolysis reactor designs investigated for commercial production of condensable tars from biomass, the fluidized bed reactor is potentially efficient due to the high particle heating rates that can be achieved (e.g. Scott et al. [22]) and its excellent mixing properties. Although the process has received considerable attention experimentally (e.g. Scott and Piskorz [20],[21]), currently there are no fundamental theoretical analyses available, addressing simultaneously all physico-chemical processes in the reactor. Most of the work to date related to fluidized bed reactors has focused on single-particle pyrolysis in a gas stream which requires *a priori* knowledge of ambient gas flow parameters, its temperature in particular (Miller and Bellan [16], Di Felice et al. [5]).

Simulation details

The reactor standard size is $0.1m \times 0.55m$ (see Fig. 1), and it is filled with sand only up to a height of $0.163\ m$ at a volume fraction of 0.6 which corresponds to dense packing. The geometry has been chosen to resemble that used in experiments by Scott and Piskorz [20],[21], among others. In the simulations, the biomass is fed through an inlet section in one of the side walls, together with an amount of gas, which preheats the biomass during the feeding process. The center of feed point 1 is located 4.6 cm from the bottom of the bed and has a height (area) of 1.86 cm; feeder no. 2 has the same height (area) and is located 12.1 cm from the bottom. In the present simulations, the temperature of the gas used for fluidization, T_g, is equal to that of the flow fed through the biomass feed section. In a previous study [14], different feedstock has been simulated by varying the cellulose/hemicellulose/lignin proportions, however, for the purpose of assessing model assumptions, only simulations with bagasse (whose composition is 36% cellulose, 47% hemicellulose and 17% lignin) are considered. This strategy is justified by the insensitivity of the results to the feedstock under consideration [14]. The initial diameter of the biomass particles is uniform in each simulation and is here varied from 0.5 to 1.0 mm, which are common values in practical operation; the sand particles have a constant diameter of 0.5 mm. Biomass particles are assumed to have an initial porosity of 0.7 (c.f. Miller and Bellan [16]) and the biomass feed flux is constant and has a value of 0.5 kg/m^2s. The gas velocity through the feeder is 0.5 m/s, and the gas flow used for fluidization of the mixture is 0.5 m/s and is uniform over the bottom of the domain. The initial temperature of biomass is 400 K whereas the initial temperature of the gas is 750 K.

Assessment of model assumptions

Collisional model assumptions

In the derivation of the model, several assumptions have been made. Here we assess three of these assumptions, all related to the derivation of the stress tensors and the granular conductivity.

The particle hydrodynamics model is a so-called 'dry' granular model where the effects of the surrounding gas on the stress tensor and granular conductivity is neglected. For this assumption to be correct, the ratio of a representative collision time scale should be small compared to the particle relaxation time scale. This assumption can be now assessed using the results of the simulation. The gas-particle relaxation time is given by $\tau_{i,12}$, given by eq. 10. On the other hand, the average collision time for a particle of class i to collide with a particle of class k is given by the expression $1/\tau_{c,ik} = n_k h_{ik} \sigma_{ik}^2 \sqrt{8\pi(\Theta_i + \Theta_k)}$ (under the assumption of small relative velocity between the two classes). As the dynamics of the bed is dominated by the motion of the sand, the ratio $\tau_{c,ss}/\tau_{s,12}$ is taken as a representa-

tive measure of the validity of the dry granular flow assumption. Fig. 2 shows this ratio as a function of the sand volume fraction for each grid point in the bed at 5 s.. The results indicate that this ratio decreases as the particle volume fraction increases, as expected. The results further indicate that for all but the very dilute regions, the collision time is smaller than the particle relaxation time, confirming the validity of the dry granular flow model that constitutes one of the elements upon which the stress relations are based. If the threshold for the validity of the dry granular flow is considered to be $\tau_{c,ss}/\tau_{s,12} < 0.1$, then it is clear that in all regions where $\alpha_s > 0.15$ the dry granular flow assumption holds. To explore in which regions the assumption may be invalid, the α_s distribution at 5 s of physical time is depicted in Fig. 3. In all regions of the reactor except around the void particle regions named "bubbles", the dry granular flow assumption holds. One could argue that for the present application focused on tar production, very little tar evolves from a low particle volume fraction region, and therefore the dry granular flow assumption is indeed very appropriate. Although this assumption evaluation is based on a single realization and at a specified physical time, the parametric study performed elsewhere [14] indicates that the results are typical.

To simplify the coding, cross derivatives are eliminated from the granular energy equations by assuming that for the purpose of calculating granular thermal conductivities and viscosities, the granular energies obey the equidistribution law; however, solutions are still obtained separately for each granular energy corresponding to a size class. This procedure simplifies the numerical solution procedure and retains the possibility of having granular temperatures that are out of equilibrium since the assumption is invoked only for the purpose of calculating the transport terms. To test this assumption, the ratio $(m\Theta)_s/(m\Theta)_b$, representing the deviation from equipartition, has been plotted in Fig. 4 at a physical time of 5s as function of the sand volume fraction and for each grid point in the numerical domain. The results show that for the dense regime this ratio is indeed close to unity, confirming the assumption that equipartition holds approximately. For the more dilute regime, the deviations from equipartition become larger. Noteworthy, the equipartition assumption holds in the regime where the dry granular assumption is valid, making the two assumptions consistent.

Finally, it is of interest to examine the assumption of small relative velocity between the two particle classes as it was used to estimate the collision integrals which yielded the form of the granular constitutive relations and the granular transport properties; see Lathouwers and Bellan [14] for details. We note that, to our knowledge, only Gourdel et al. [8] calculated these collision integrals without the benefit of this assumption, but only for the simple case of homogeneous flow. Depicted in Fig. 5 is the ratio $z = 0.75(\Delta u_{ik})^2/[3/2 \times (\Theta_s + \Theta_b)]$. Clearly, at most locations within the very dense particle regime the assumption $z < 1$ is satisfied, however, this hypothesis is not reliable unless $\alpha_s > 0.4$. The regime $z \ll 1$ is confined to an even higher particle volume fraction regime. For small α_s, particularly for $\alpha_s < 0.25$, the small drift velocity assumption is inappropriate.

The above discussion shows that the basis for the granular stress and conductivity models is firm in the very dense particle regime which is of interest for the present application as it is the one dominating tar production. The small drift velocity assumption must though be reconsidered for dense, moderate and small volume fraction regimes, and should make the subject of future studies.

Heat transfer assumptions

Heat transfer is a process governing the biomass temperature rise and the ensuing evolution of tar; see Lathouwers and Bellan [14] for details. Heat transfer is here of two types: conductive and radiative. The importance of the radiative heat transfer has been assessed by Lathouwers and Bellan [15], and it was found to have a non-negligible contribution. Here we evaluate some elements of the conductive heat transfer model. As shown in eq. 16, a blowing factor correction whose expression is given by eq. 17 is incorporated in the calculation of the Nusselt number. To investigate the importance of this correction, the blowing factor has been extracted from several simulations differing by the initial biomass particle size. Table 4 lists the minimum value of F_{bl} throughout the domain at $t = 5$ s. Clearly, for all cases investigated the blowing effect significantly reduces the heat transfer to the particles (up to 40% in the large diameter case). This means that neglecting this correction could give overly optimistic results concerning conversion rates of biomass to tar.

Another simplifying assumption made in modeling the heat transfer to the particles is that the resistance to heat transfer is mainly at the surface of the particles (see Lathouwers and Bellan [14]), i.e. the Biot number, Bi, is assumed small. This assumption is consistent with the further requirement of the Eulerian volume averaging approach combined with the Lagrangian tracking of the particle thermodynamic energy on its trajectory through the use of its mean temperature only. Table 4 further lists values of Bi encountered for simulations initiated with several initial biomass particle size. The results indicate that the range of Biot numbers encountered for the biomass particles is independent of initial particle size. Furthermore, Bi is below unity, indicating the approximate applicability of the particle heating theory. We note however that Bi is not $\ll 1$, showing that internal heat transfer may also play a role. An inquiry about the validity of the small Bi assumption for the sand particles reveals that Bi is approximately 10 times larger than for biomass (10 times lower thermal conductivity). This is however of no concern, as the sand temperature quickly becomes close to that of the gas (see Lathouwers and Bellan [14]), which then renders the heat transfer model marginally important, regardless of the specific heat transfer correlation.

Conclusions

Several assumptions made in the development of a comprehensive mathematical model describing the evolution of a granular flow in a fluidized bed reactor have been assessed. The fluidized bed reactor consists of a cylindrical vessel filled with sand which is fluidized by injecting a (relatively hot) flow of nitrogen through its porous bottom plate; the sand is initially at room temperature and heats up by contact with the

hotter nitrogen flow. Fresh biomass, introduced through one side of the reactor, heats up and pyrolyses. The specific application under consideration is the production and harvesting of tar from biomass pyrolysis for hydrogen production. The model is based on detailed submodels for the hydrodynamics of the gas-solid mixture and the biomass kinetics. The separately validated biomass pyrolysis kinetics model of Miller and Bellan [16] was chosen for its ability to differentiate between the various biomass feeds available through the use of a superimposed cellulose, hemicellulose and lignin kinetics scheme. The hydrodynamics model is based on the detailed multiphase model of Lathouwers and Bellan [14] which describes the dynamics and heat transfer of dense, reactive gas-solid mixtures. The multiphase flow mathematical description is obtained from systematic averaging of the local instantaneous equations using the kinetic theory of granular flows in combination with rigid sphere interaction models explicitly accounting for collisional transfer between the particles. The isothermal model was previously validated using experimental data (see Lathouwers and Bellan [13]).

In this study, we used results from some of the extensive simulations of Lathouwers and Bellan [14] to evaluate, on an *a posteriori* basis, assumptions related to the derivation of the granular stress model, including the granular conductivities and viscosities, and also assumptions pertaining to the heat transfer model. Examination of these assumptions showed that the small particle drift approximation (i.e. small difference between velocities of the two particle classes) is not met, except in the very high volume fraction particle regime. This points out that new strategies must be developed in calculating the collision integrals which are the basis of the granular flow constitutive relations and transport coefficients. However, under the small drift assumption, both the dry granular flow assumption and the equipartition of granular energy assumption used uniquely for the calculation of transport coefficients were valid in the high volume ratio regime which is of most interest for the present application. The heat transfer model was shown to be approximately justified by the smaller than unity Biot number for the biomass; however, the Biot number is not much smaller than unity, showing that internal processes may also play a role. Finally, it was shown that the blowing factor introduced to correct for the reduction in heat transfer due to mass evolution form the particle is indeed smaller than unity, indicating that this correction is truly necessary.

Acknowledgments

This research was sponsored by the U.S. Department of Energy (DOE), with Mr. Neil Rossmeissel (DOE Headquarters) and Mr. D. Hooker (DOE Golden Center) serving as contract monitors, under an agreement with the National Aeronautics and Space Administration. Computational resources were provided by the supercomputing facility at JPL.

1. Anderson, K. G. and Jackson, R., *J. Fluid Mech.* **1992**. A comparison of the solutions of some proposed equations of motion of granular materials for fully developed flow down inclined planes. 241, 145-168.
2. Barrett, R., Berry, M., Chan, T. F., Demmel, J., Donato, J., Dongarra, J., Eijkhout, V., Pozo, R., Romine, C. and Van der Vorst, H., **1994**. Templates for the solution of linear systems: building blocks for iterative methods. SIAM, Philadelphia.
3. Brown, P. N., Byrne, G. D. and Hindmarsh, A. C., *SIAM J. Sci. Stat. Comput.* **1989**. VODE: A Variable-coefficient ODE solver. 10(5), 1038-1051.
4. Campbell, C. S., *Ann. Rev. Fluid Mech.* **1990**. Rapid granular flows. 22, 57-92.
5. Di Felice, R., Coppola, G., Rapagna, S., and Jand, N., *The Can. J. Chem. Eng.* **1999**. Modeling of biomass devolatilization in a fluidized bed reactor. 77, 325-332.
6. Drew, D. A., *Ann. Rev. Fluid Mech.* **1983**. Mathematical modeling of two-phase flow. 15, 261-291.
7. Gidaspow, D., *Appl. Mech. Rev.* **1986**. Hydrodynamics of fluidization and heat transfer: supercomputer modelling. 39, 1-22.
8. Gourdel, C., Simonin, O. and Brunier, E., **2000**. Eulerian Modelling of binary mixtures of colliding particles and validation from Lagrangian tracking coupled to Large Eddy Simulation of homogeneous gas-solid turbulent flow. Submitted to Int. J. Multiphase Flow.
9. Gyarmathy, G., *Multiphase Science and Technology* **1982**. The spherical droplet in gaseous carrier streams: review and synthesis. Vol. 1. Eds. Hewitt, G. F., Delhaye, J. M., and Zuber, N. McGraw Hill, 99-279.
10. Jenkins, J. T. and Mancini, F., *J. Appl. Mech.* **1987**. Balance laws and constitutive relations for plane flows of a dense, binary mixture of smooth, nearly elastic, circular disks. 54, 27-34.
11. Lathouwers, D., **1999**. Modelling and Simulation of Turbulent Bubbly Flows. PhD thesis, Delft University of Technology, The Netherlands.
12. Lathouwers, D. and Bellan, J., **1999**. Multiphase flow equations for modeling tar production from biomass particle pyrolysis in a fluidized bed reactor. Fall Technical Meeting of the Western States Section of the Combustion Institute, Irvine, October 25-26.
13. Lathouwers, D. and Bellan, J., *Proc. of the Comb. Inst.* **2000**. Modeling and simulation of bubbling fluidized beds containing particle mixtures, Vol. 28, 2297-2304
14. Lathouwers, D. and Bellan, J., *Int. J. Multiphase Flow.* **2001**. Modeling of dense gas-solid reactive mixtures applied to biomass pyrolysis in a fluidized bed. submitted
15. Lathouwers, D. and Bellan, J., *Energy and Fuels.* **2001**. Yield optimization and scaling of fluidized beds for tar production from biomass. submitted
16. Miller, R. S. and Bellan, J., *Combust. Sci. and Tech.* **1997**. A generalized biomass pyrolysis model based on superimposed cellulose, hemicellulose and lignin kinetics.126, 97-137.
17. Miller, R. S. and Bellan, J., *Energy and Fuels* **1998**. Nu-

merical simulation of vortex pyrolysis reactors for condensable tar production from biomass. 12(1), 25-40.

18. Miller, R. S., Harstad, K. and Bellan, J., *Int. J. Multiphase Flow* **1999**. Evaluation of equilibrium and non-equilibrium evaporation models for many-droplet gas-liquid flow simulations. 24(6), 1025-1055.
19. Schiller, L. and Nauman, A., *V.D.I. Zeitung* **1935**. A drag coefficient correlation. 77, 318-320.
20. Scott, D. S. and Piskorz, J., *Can. Journal Chem Eng.***1982**. The flash pyrolysis of Aspen-polar wood. 60, 666-674.
21. Scott, D. S. and Piskorz, J., *Can. Journal Chem Eng* **1984**. The continuous pyrolysis of biomass.62, 404-412.
22. Scott, D. S., Majerski, P., Piskorz, J., and Radlein, D., *J. Anal. Appl. Pyrolysis* **1999**. A second look at fast pyrolysis of biomass - the RTI process. 51, 23-37.
23. Strang, G., *SIAM J. of Numer. Anal.* **1968**. On the construction and comparison of difference schemes. 5(3), 506-517
24. Zaichik, L. I., Pershukov, V. A., Kozelev, M. V., and Vinberg, A. A., *Exp. Thermal Fluid Sci.* **1997**. Modeling of dynamics, heat transfer, and combustion in two-phase turbulent flows: 2. Flows with heat transfer and combustion. 15, 311-322.

Reaction	$A(1/s)$	$E(J/kmol)$
K_1^c	2.8×10^{19}	242.4×10^6
K_2^c	3.28×10^{14}	196.5×10^6
K_3^c	1.30×10^{10}	150.5×10^6
K_1^h	2.10×10^{16}	186.7×10^6
K_2^h	8.75×10^{15}	202.4×10^6
K_3^h	2.60×10^{11}	145.7×10^6
K_1^l	9.60×10^8	107.6×10^6
K_2^l	1.50×10^9	143.8×10^6
K_3^l	7.70×10^6	111.4×10^6
K_4	4.28×10^6	108×10^6

Table 1: Rate constants and activation energy for the biomass pyrolysis kinetics scheme. The char formation ratios for reaction K_3 are: $X^c = 0.35$, $X^h = 0.60$, and $X^l = 0.75$.

Species	W	C_p	$\lambda \times 10^2$	$\mu \times 10^5$	$D \times 10^4$
N_2	28.013	1120.91	5.63	3.58	8.52
Gas	30	1100	2.577	3.0	1.1
Tar	100	2500	2.577	3.0	1.1

Table 2: Property values for the gas phase species. The properties for nitrogen are taken at $T = 800K$ and $p = 100kPa$. Units are as follows: $W(kg/kmol)$; $C_p(J/kgK)$; $\lambda(J/msK)$; $\mu(kg/ms)$; and $D(m^2/s)$.

Species	$C_p(J/kgK)$	$\rho(kg/m^3)$
Biomass	2300	2167
Char	1100	2333
Sand	800	2600

Table 3: Specific heat and densities for solid species. Biomass refers to both virgin species and active species. The densities are the intrinsic values, not accounting for the pores.

$d_p(mm)$	F_{bl}	Bi(biomass)
0.5	0.75	$0.10 - 0.25$
0.75	0.69	$0.08 - 0.30$
1.0	0.60	$0.08 - 0.34$

Table 4: Minimum blowing factor encountered in domain and range of Biot numbers encountered for the biomass particles for different biomass particle diameters.

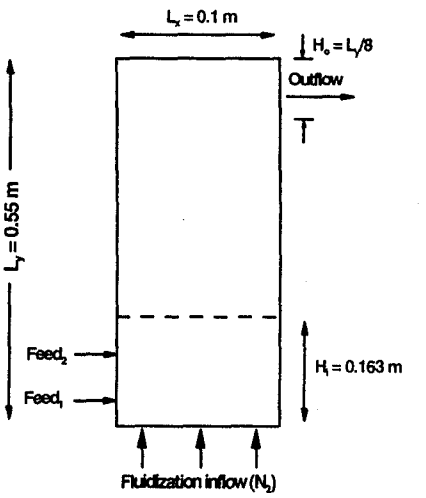

Figure 1: Schematic of the fluidized bed.

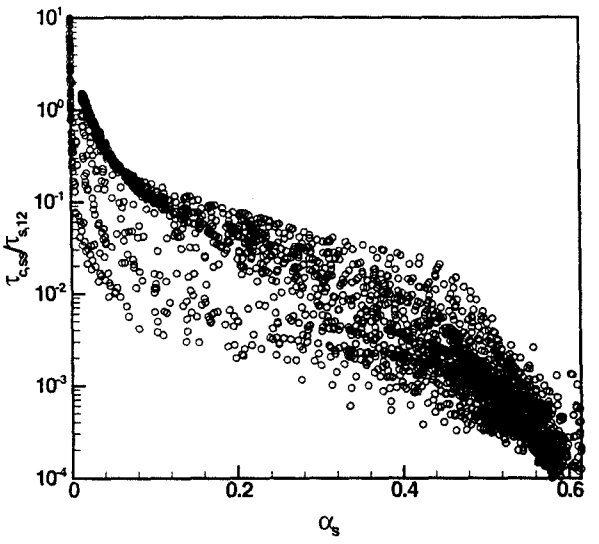

Figure 2: Ratio of the gas-particle and the collisional timescale as function of the particle volume fraction at all grid locations at $t = 5$s.

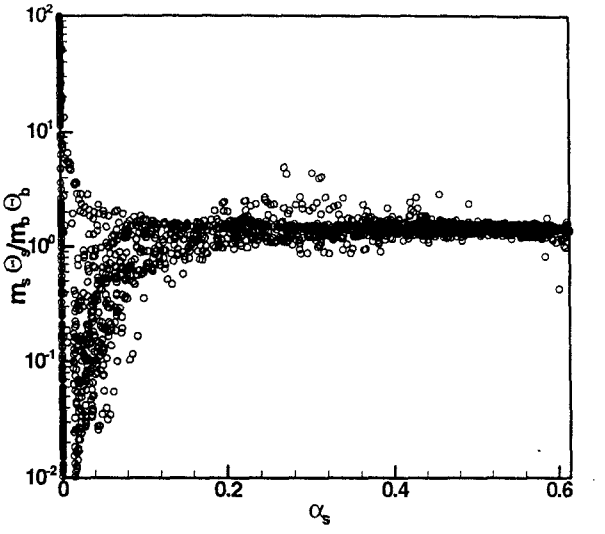

Figure 4: Equilibration ratio $m_s\Theta_s/m_b\Theta_b$ as function of the particle volume fraction in the bed at all grid locations at $t = 5$ s.

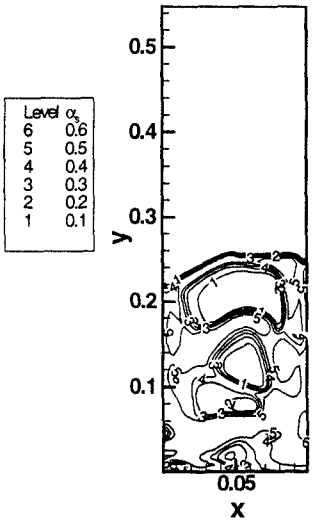

Figure 3: Volume fraction of solids at $t = 5$ s.

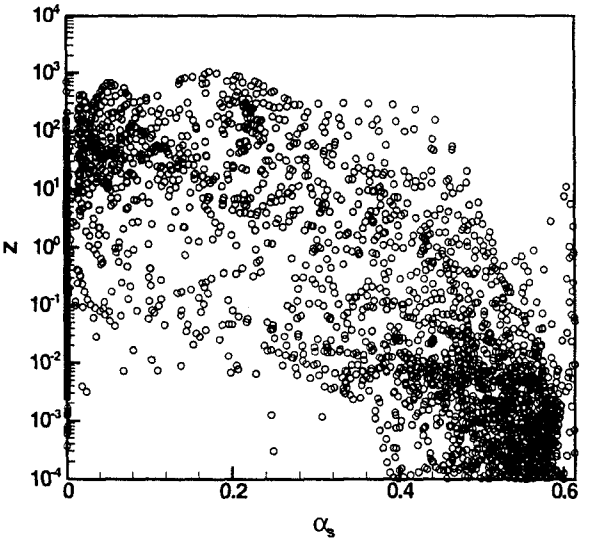

Figure 5: Ratio between the drift velocity of the two particle classes, and an average granular energy of the particles at all grid locations at $t = 5$ s.